The Journal of Chemical Physics

RESEARCH ARTICLE | APRIL 08 2025

High-resolution photoelectron spectroscopy of cryogenically cooled SiC^-

Shuaiting Yan ; Jiayi Chen; Rui Zhang ; Wenru Jie; Chuangang Ning

J. Chem. Phys. 162, 144308 (2025)
https://doi.org/10.1063/5.0265504

The Journal of Chemical Physics ARTICLE pubs.aip.org/aip/jcp

High-resolution photoelectron spectroscopy of cryogenically cooled SiC^-

Cite as: J. Chem. Phys. 162, 144308 (2025); doi: 10.1063/5.0265504
Submitted: 14 February 2025 • Accepted: 20 March 2025 •
Published Online: 8 April 2025

Shuaiting Yan, Jiayi Chen, Rui Zhang, Wenru Jie, and Chuangang Ning[a)]

AFFILIATIONS

Department of Physics, State Key Laboratory of Low Dimensional Quantum Physics, Frontier Science Center for Quantum Information, Tsinghua University, Beijing 100084, China

[a)]Author to whom correspondence should be addressed: ningcg@tsinghua.edu.cn

ABSTRACT

We report high-resolution photoelectron spectroscopy of SiC^- anions using a cryogenic ion trap combined with the slow-electron velocity-map imaging method. Photodetachment transitions to the neutral SiC ground state X $^3\Pi$ and excited states (a $^1\Sigma^+$, b $^1\Pi$) were observed, revealing the fine structure of the X $^3\Pi$ band. A long-lived excited state (A $^3\Pi$) of SiC^- was observed at 3380(101) cm^{-1} above the anionic ground state. The electron affinity (EA) was determined as EA(SiC) = 19 327(15) cm^{-1} or 2.396(2) eV. The spectroscopic constants of the ground state (X′ $^2\Sigma^+$) of SiC^- were derived as ω_e = 1016(21) cm^{-1} and $\omega_e x_e$ = 5.20(22) cm^{-1}.

I. INTRODUCTION

Carbon and silicon are fundamental elements in interstellar chemistry, and diatomic SiC molecules have been observed in carbon-rich stars, stellar atmospheres, and interstellar molecular clouds.[1–3] Beyond astrophysical chemistry, SiC is widely utilized in semiconductor devices and advanced ceramics owing to its exceptional thermal and electronic properties.[4–8] Spectroscopic characterization of SiC is critical for understanding SiC-based materials in diverse environments.[9–21]

In 1988, Bernath *et al.* produced gas-phase SiC molecules using a composite-wall hollow cathode for the first time. Their work identified the 0–0 band of the $d\ ^1\Sigma^+$–$b\ ^1\Pi$ electronic transition of SiC through Fourier-transform emission spectroscopy combined with *ab initio* calculations.[22] Subsequent infrared emission studies resolved the A $^3\Sigma^-$–X $^3\Pi$ transition, yielding molecular constants for these states.[10,23] Later, Ebben *et al.* employed pulsed-laser vaporization with supersonic cooling to generate SiC radical, probing seven rovibronic bands of the C $^3\Pi$ (v' = 0–6) − X $^3\Pi$ (v'' = 0) transition via laser-induced fluorescence spectroscopy.[24,25] Butenhoff and Rohlfing further determined vibrational term energies and rotational constants for higher vibrational states (v' = 0–8 in C $^3\Pi$, v'' = 0–5 in X $^3\Pi$).[26] The rotational constants of ground-state SiC (X $^3\Pi$) were precisely measured using millimeter-wave rotational spectroscopy,[27] while its fundamental vibrational frequency ν_0 = 953.320 62(27) cm^{-1} was obtained via CO_2-Faraday laser magnetic resonance (LMR) spectrometer.[28] Recent synchrotron studies further established the first ionization potential of SiC as 8.978(10) eV.[29]

Theoretical efforts have paralleled experimental advances.[30–36] Initial studies predicted low-lying states of SiC: X $^3\Pi$, A $^3\Sigma^-$, a $^1\Sigma^+$, B $^3\Sigma^+$, and C $^3\Pi$,[37–39] while subsequent work explored singlet, triplet, and quintet states, providing excitation energies (T_e), equilibrium internuclear distances (r_e), dissociation energies (D_e), and spectroscopic constants (ω_e) for these new electronic states.[40,41] Shi *et al.* calculated potential energy curves (PECs) for 25 Λ–S and 20 Ω states, incorporating spin–orbit coupling (SOC) effect to achieve remarkable agreement with experimental data.[42] Recently, Zhang and Wang calculated vibronic emissions of SiC between its different singlet states to enhance the experimental spectral analysis.[43] The latest calculations of the vibrational constants (ω_e, $\omega_e x_e$) and other molecular constants (D_e, r_e, B_e, α_e) for SiC (X $^3\Pi$) were reported by Fan *et al.* using the high-level variational algebraic method (VAM).[44]

In contrast to neutral SiC, studies on SiC^- anion are relatively rare. Early theoretical work by Anglada *et al.* identified two bound states ($^2\Sigma^+$ and $^2\Pi$) and estimated an electron affinity (EA) of 1.98 eV using multi-reference single and double excitation configuration interaction (MRD–CI) calculations.[45] Subsequent studies predicted potential energy curves and spectroscopic constants of

SiC^-,[46,47] while neon matrix isolation experiments by Grutter *et al.* revealed A $^2\Pi \leftarrow X\ ^2\Sigma^+$ and B $^2\Sigma^+ \leftarrow X\ ^2\Sigma^+$ transitions at 5 K.[48] SiC^- has also been proposed as a candidate for laser cooling of negative ions.[49,50] Compared to its isoelectronic species C_2^-, the polar SiC^- may have the advantage of repumping via vibrational spectroscopic techniques since it has nonzero dipole moment.

Here, we present high-resolution photoelectron spectra of a cryogenically cooled SiC^- using the slow-electron velocity-map imaging (SEVI) method. This technique resolves the fine structure in the photodetachment channel SiC ($X\ ^3\Pi$) ← SiC^- ($X'\ ^2\Sigma^+$), enabling precise determination of the electron affinity of SiC. In addition, a long-lived excited state (A $^2\Pi$) of SiC^- was observed.

II. EXPERIMENTAL AND THEORETICAL METHODS

The experiments employed a cryogenically slow-electron velocity-map imaging (cryo-SEVI) apparatus, comprising four key components: (1) a laser vaporization ion source, (2) a cold octupole radio frequency (rf) ion trap, (3) a time-of-flight (TOF) mass spectrometer, and (4) a photoelectron velocity-map imaging system.

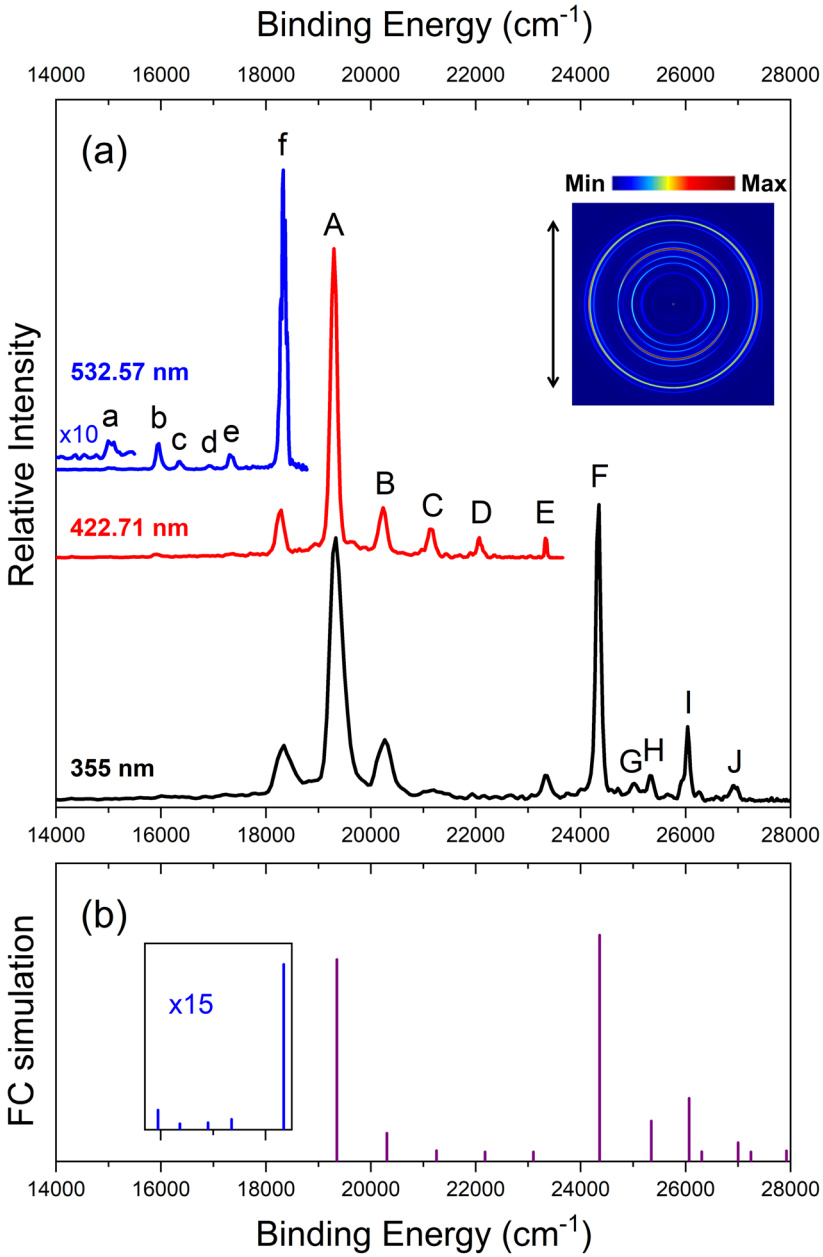

FIG. 1. (a) Photoelectron spectrum SiC^-. The weak peak *a* is multiplied by a factor of 10. The inset image is at a photon wavelength of 355 nm. (b) The purple and blue vertical sticks represent the Franck–Condon simulations. The inset shows a series of simulations from the hot band of the anionic ground state ($X'\ ^2\Sigma^+$) and a metastable state ($A\ ^2\Pi$) to $X\ ^3\Pi$. The blue vertical sticks represent the weak simulated peaks (*b–f*), scaled by a factor of 15.

The detailed descriptions of this setup are available in previous studies.[51–53] SiC^- anions were generated by ablating a rotating and translating Si/C disk target (13 mm diameter, carborundum) with 532 nm pulses from an Nd: YAG laser (20 Hz, ~10 mJ/pulse). The nascent anions, entrained in helium gas at a backing pressure of 3 bar, were guided through a hexapole ion guide into a cryogenic radio frequency (RF) ion trap mounted on a helium refrigerator. (5–300 K). Within the trap, ions were cooled via collisions with a buffer gas mixture (20% H_2 and 80% He) for 45 ms.[28] SiC^- anions were mass-selected via a Wiley–McLaren type time-of-flight (TOF) mass spectrometer[54] and intercepted by a detachment laser in the interaction region of velocity map imaging (VMI).[55] Photodetachment laser was from an optical parametrical oscillator (OPO, 210–709 nm, linewidth ~6 cm^{-1}), pumped by an Nd: YAG laser operating at 20 Hz. The photodetached electrons were projected onto a set of micro-channel plates coupled with a phosphor screen and images were captured by a charge-coupled device (CCD) camera. The VMI energy calibrations were conducted using the known spectra of $^{28}Si^-$ for the threshold photodetachment.[56–59] The well-known spectra of NO_2^- were also used for the energy calibration for the overview spectrum since NO_2^- has many sharp lines distributed in a large energy range.[60–63] The projected 2D photoelectron image was reconstructed into 3D photoelectron distribution using the maximum entropy velocity Legendre reconstruction (MEVELER) method,[64] yielding the electron energy distributions.

Electronic configurations of electronic states of SiC^- were computed using Becke's three-parameter and Lee–Yang–Parr's (B3LYP) gradient-corrected correlation hybrid functional[65,66] with the 6−311++G(d, p) basis set[67] via the Gaussian program package.[68] Molecular orbital (MO) contours were visualized using the visual molecular dynamics (VMD) program.[69]

III. RESULTS AND DISCUSSION

A. High-resolution photoelectron spectra

Figure 1 shows the photoelectron image at 355 nm and photoelectron spectra at 355, 422.71, and 532.57 nm with an imaging voltage of −650 V, along with the Franck–Condon simulation. Table I lists the binding energies of these peaks, shifts from the band origin, anisotropic parameter (β) values, and their assignment. β can provide valuable information for spectral assignments since it depends on the shape and symmetry of the photodetached anionic molecular orbital (MO).[70–72] Based on the measured β values and previously reported theoretical calculations of $SiC^{-/0}$,[42,47] all peaks in Fig. 1(a) can be assigned. Peak *A* was assigned to the photodetachment channel from the anionic ground state $X'\ ^2\Sigma^+$ ($v' = 0$) to the neutral ground state $X\ ^3\Pi_2$ ($v = 0$), which defines the electron affinity of SiC. Peaks *F* and *I* are the $0 \leftarrow 0$ transitions from the anionic ground state to the two neutral excited states $a\ ^1\Sigma^+$ and $b\ ^1\Pi$, respectively. The term energies of $a\ ^1\Sigma^+$ and $b\ ^1\Pi$ were determined to be 5032(48) and 6737(38) cm^{-1}, respectively, based on their energy gaps. These values are in reasonable agreement with previously calculated values of 4831 and 6628 cm^{-1}.[42]

Interestingly, several weak peaks *a*–*f* were observed before peak *A*. Our cold ion trap usually cools all electronically and vibrationally excited states down to their ground states. A possible explanation for these peaks is either contamination by other negative ions of the same mass or the presence of excited states with long lifetimes, which cannot be effectively quenched by collisions with the buffer

TABLE I. Peak positions, shifts from origin, and assignments, along with their anisotropic parameters (β) values for SiC^- photoelectron spectra.

Peak	EBE (cm^{-1})	Shift from origin (cm^{-1})	Assignment	β value[a]
a	15 051(191)	−4300	$X\ ^3\Pi\ (v = 0) \leftarrow A\ ^2\Pi\ (v' = 1)$	1.412
b	15 947(96)	−3404	$X\ ^3\Pi\ (v = 0) \leftarrow A\ ^2\Pi\ (v' = 0)$	1.473
c	16 353(100)	−2998	$X\ ^3\Pi\ (v = 0) \leftarrow X'\ ^2\Sigma^+\ (v' = 3)$	−0.226
d	16 926(116)	−2425	$X\ ^3\Pi\ (v = 1) \leftarrow A\ ^2\Pi\ (v' = 0)$	0.949
e	17 332(122)	−2019	$X\ ^3\Pi\ (v = 0) \leftarrow X'\ ^2\Sigma^+\ (v' = 2)$	−0.371
f	18 333(127)	−1018	$X\ ^3\Pi\ (v = 0) \leftarrow X'\ ^2\Sigma^+\ (v' = 1)$	−0.674
A	19 351(130)	0	$X\ ^3\Pi\ (v = 0) \leftarrow X'\ ^2\Sigma^+\ (v' = 0)$	−0.679
B	20 271(180)	920	$X\ ^3\Pi\ (v = 1) \leftarrow X'\ ^2\Sigma^+\ (v' = 0)$	−0.636
C	21 191(127)	1840	$X\ ^3\Pi\ (v = 2) \leftarrow X'\ ^2\Sigma^+\ (v' = 0)$	−0.371
D	22 074(65)	2723	$X\ ^3\Pi\ (v = 3) \leftarrow X'\ ^2\Sigma^+\ (v' = 0)$	−0.551
E	23 335(51)	3984	$a\ ^1\Sigma^+\ (v = 0) \leftarrow X'\ ^2\Sigma^+\ (v' = 1)$	1.315
F	24 359(38)	5008	$a\ ^1\Sigma^+\ (v = 0) \leftarrow X'\ ^2\Sigma^+\ (v' = 0)$	1.408
G	25 021(106)	5670	$b\ ^1\Pi\ (v = 0) \leftarrow X'\ ^2\Sigma^+\ (v' = 1)$	−0.083
H	25 343(68)	5992	$a\ ^1\Sigma^+\ (v = 1) \leftarrow X'\ ^2\Sigma^+\ (v' = 0)$	1.101
I	26 064(23)	6713	$b\ ^1\Pi\ (v = 0) \leftarrow X'\ ^2\Sigma^+\ (v' = 0)$	−0.411
J	26 922(173)	7571	$b\ ^1\Pi\ (v = 1) \leftarrow X'\ ^2\Sigma^+\ (v' = 0)$	−0.412

[a]β values of peaks *a*–*e* were recorded at a wavelength of 532.57 nm, β values of peaks *f*–*D* at 422.71 nm, and β values of peaks *E*–*J* at 355 nm.

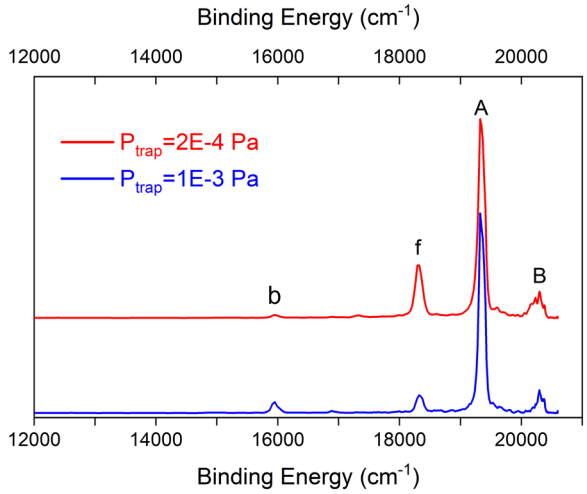

FIG. 2. Photoelectron spectra of SiC^- measured with low buffer gas pressure (P_{trap} = 2 × 10^{-4} Pa, red curve) and high buffer gas pressure of the ion trap (P_{trap} = 1 × 10^{-3} Pa, blue curve) at photon energy $h\nu$ = 20 595 cm^{-1}.

gas. To test these possibilities, we varied the buffer gas density in the ion trap and observed the changes of in the intensity of these peaks. As shown in Fig. 2, when the buffer gas increased (with the background pressure rising from 2 × 10^{-4} to 1 × 10^{-3} Pa), the intensity of peak *f* decreases significantly while peak *b* increases. Therefore, it is reasonable to assign peaks *a*–*f* to excited states with long lifetimes rather than contamination, as contamination would be independent of the buffer gas density. In addition, the anisotropic parameters β for peaks *f* and *A* are roughly the same, while peak *b* shows a significantly different β value, as listed in Table I. For example, β for peak *b* is 1.473 for the photodetachment laser at 532.57 nm, while β = −0.674 for peak *f* and β = −0.679 for peak *A* at 422.71 nm. The previous experimental investigation revealed that SiC^- has an excited state A $^2\Pi$ with an energy 3556(2) cm^{-1} above its ground state, which is in reasonable agreement with our experimental result 3380 cm^{-1}.[48] Therefore, peak *b* is assigned to the transition SiC X $^3\Pi$ (v = 0) ← SiC^- A $^2\Pi$ (v' = 0), while peak *f* is assigned as a hot band of peak *A*. Because peak *b* remains observable after SiC^- has been stored in the ion trap for 45 ms; this suggests that the lifetime of A $^2\Pi$ is comparable with 45 ms.

To accurately determine the electron affinity (EA) of SiC, high-resolution photoelectron spectra were measured near the photodetachment threshold of each prominent peak, using an imaging voltage of −150 V. As shown in Fig. 3, peaks *f*, *A*, *I* exhibit fine structures. Peak *A* splits into five well-resolved peaks with roughly equal intervals (~45 cm^{-1}). Peaks *A*-3, 4, and 5 are the spin-orbital splitting results of the final neutral state X $^3\Pi$.[42] The experimental intervals of 43 and 43 cm^{-1} are in good agreement with the previous theoretical predictions for the intervals between the $^3\Pi_2$, $^3\Pi_1$, and $^3\Pi_0$ terms (36 and 36 cm^{-1}). The weak peaks *A*-1 and *A*-2 arise from transitions from the vibrational excited state (v' = 1) of the anionic ground state X′ $^2\Sigma^+$ to the vibrational excited state (v = 1) of the two SOC components ($^3\Pi_2$, $^3\Pi_1$). Peak *f* displays a splitting structure similar to that of peak *A*, originating from the vibrationally excited state of the

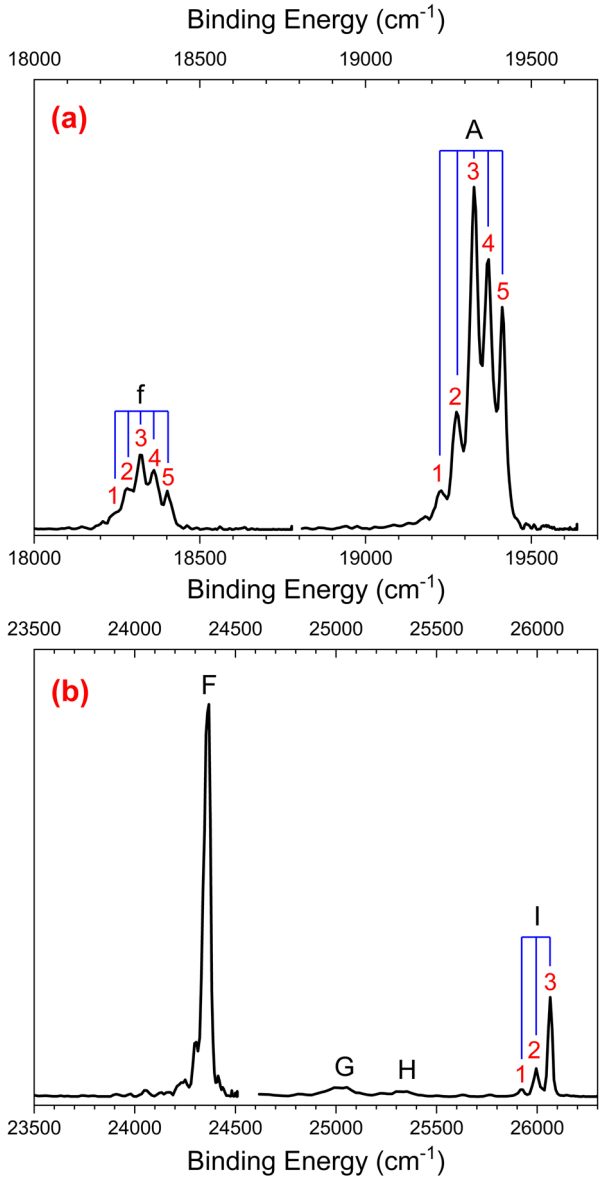

FIG. 3. Fine structures of peaks *f*, *A*, and *I*.

anionic ground state X′ $^2\Sigma^+$. The fundamental vibrational frequency of SiC^- in its electronic ground state (X′ $^2\Sigma^+$) was determined to be 1006(21) cm^{-1}. The EA value of SiC was further precisely determined to be 19 327(15) cm^{-1} or 2.396(2) eV, while the excited state (A $^2\Pi$) is 3380(101) cm^{-1} above the ground state.

For peaks *F* and *I*, the neutral final state of the photodetachment transition corresponds to a singlet state (a $^1\Sigma^+$, b $^1\Pi$), meaning that the spin–orbital splitting should be absent. Upon careful analysis, the fine structure of peak *I* was attributed to transitions from the vibrational excited states (v' = 1, 2) of the anion ground state X′ $^2\Sigma^+$ to corresponding vibrationally excited states (v = 1, 2) of the neutral excited state b $^1\Pi$. In contrast to peak *I*, no fine structure

TABLE II. Fine structures of peaks *f*, *A*, and *I* for SiC^-. The shift column is the energy relative to the onset peak of the respective fine structures.

Peaks	Label	Measured binding energy (cm^{-1})[a]	Shift (cm^{-1})	Assignment
f	1	18 244(28)	0	$X\ ^3\Pi_2\ (v=1) \leftarrow X'\ ^2\Sigma^+\ (v'=2)$
	2	18 284(17)	40	$X\ ^3\Pi_1\ (v=1) \leftarrow X'\ ^2\Sigma^+\ (v'=2)$
	3	18 321(15)	77	$X\ ^3\Pi_2\ (v=0) \leftarrow X'\ ^2\Sigma^+\ (v'=1)$
	4	18 361(17)	117	$X\ ^3\Pi_1\ (v=0) \leftarrow X'\ ^2\Sigma^+\ (v'=1)$
	5	18 404(15)	160	$X\ ^3\Pi_0\ (v=0) \leftarrow X'\ ^2\Sigma^+\ (v'=1)$
A	1	19 224(18)	0	$X\ ^3\Pi_2\ (v=1) \leftarrow X'\ ^2\Sigma^+\ (v'=1)$
	2	19 277(19)	54	$X\ ^3\Pi_1\ (v=1) \leftarrow X'\ ^2\Sigma^+\ (v'=1)$
	3	19 327(15)	103	$X\ ^3\Pi_2\ (v=0) \leftarrow X'\ ^2\Sigma^+\ (v'=0)$
	4	19 370(16)	146	$X\ ^3\Pi_1\ (v=0) \leftarrow X'\ ^2\Sigma^+\ (v'=0)$
	5	19 413(14)	189	$X\ ^3\Pi_0\ (v=0) \leftarrow X'\ ^2\Sigma^+\ (v'=0)$
I	1	25 923(13)	0	$b\ ^1\Pi\ (v=2) \leftarrow X'\ ^2\Sigma^+\ (v'=2)$
	2	25 995(28)	72	$b\ ^1\Pi\ (v=1) \leftarrow X'\ ^2\Sigma^+\ (v'=1)$
	3	26 064(23)	142	$b\ ^1\Pi\ (v=0) \leftarrow X'\ ^2\Sigma^+\ (v'=0)$

[a]The uncertainty of the measurement is given in the parentheses.

was observed for peak *F*, likely because the harmonic vibrational constants of the $a\ ^1\Sigma^+$ state and $X'\ ^2\Sigma^+$ state are very similar, 1008 cm^{-1} vs 1016(21) cm^{-1}. The assignments of all fine structures are presented in Table II.

The infrared spectroscopy of the $A\ ^3\Sigma^-$–$X\ ^3\Pi$ transition of the SiC radical indicates that the excited state $A\ ^3\Sigma^-$ lies 3773.31(17) cm^{-1} above the ground state ($X\ ^3\Pi$).[10] In our experiments, we observed photodetachment transitions $X\ ^3\Pi \leftarrow X'\ ^2\Sigma^+$ and a $^1\Sigma^+ \leftarrow X'\ ^2\Sigma^+$, but no transition $A\ ^3\Sigma^- \leftarrow X'\ ^2\Sigma^+$ was observed. This is because the $A\ ^3\Sigma^- \leftarrow X'\ ^2\Sigma^+$ transition requires a two-electron process. Figure 4 shows the frontier molecular orbitals (FMOs) of SiC^-. The electronic configuration of $SiC^-\ X'\ ^2\Sigma^+$ is $(5\sigma)^2(6\sigma)^2(2\pi)^4(7\sigma)$, while $(5\sigma)^2(6\sigma)^2(2\pi)^2(7\sigma)^2$ for SiC $A\ ^3\Sigma^-$. For the transition $A\ ^3\Sigma^- \leftarrow X'\ ^2\Sigma^+$, considering the multiplicity and orbital symmetry, one electron from the 2π orbitals is photodetached, while the other is excited to the 7σ orbital. In principle, a transition from the first excited state $A\ ^2\Pi$ of the SiC^- anion to the neutral excited state $A\ ^3\Sigma^-$ is possible. The binding energy of this channel is expected to be ~393 cm^{-1} higher than that of the EA channel, based on the measured energy levels. Indeed, a weak band was observed at the tail of peak *A* (EA peak), which was assigned to the transition $A\ ^3\Sigma^- \leftarrow A\ ^2\Pi$.

Frontier molecular orbitals (FMOs)

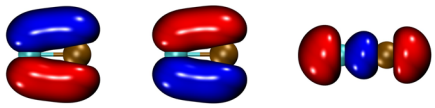

3π 4π 7σ

State	Electronic Configuration
$SiC^-\ (X'\ ^2\Sigma^+)$	$(5\sigma)^2(6\sigma)^2(3\pi)^2(4\pi)^2(7\sigma)$
$SiC^-\ (A\ ^2\Pi)$	$(5\sigma)^2(6\sigma)^2(3\pi)^2(4\pi)(7\sigma)^2$
$SiC\ (X\ ^3\Pi)$	$(5\sigma)^2(6\sigma)^2(3\pi)^2(4\pi)(7\sigma)$
$SiC\ (a\ ^1\Sigma^+)$	$(5\sigma)^2(6\sigma)^2(3\pi)^2(4\pi)^2$
$SiC\ (A\ ^3\Sigma^-)$	$(5\sigma)^2(6\sigma)^2(3\pi)(4\pi)(7\sigma)^2$
$SiC\ (b\ ^1\Pi)$	$(5\sigma)^2(6\sigma)^2(3\pi)(4\pi)^2(7\sigma)$

FIG. 4. Relevant frontier molecular orbital (FMO) contours and electronic configurations of $SiC^{-/0}$.

B. Franck–Condon analysis and spectroscopic constants

The electron affinity (EA) of silicon [1.389 521 2(7) eV] is higher than that of carbon [1.262 122 6(12) eV],[57,73] leading to Si^- and C being the products of the lowest-energy dissociation channel of SiC^-. The dissociation energy (D_0) of SiC^- can be calculated using the following energetic relation:

$$D_0(SiC^-) = EA(SiC) - EA(Si) + D_0(SiC), \quad (1)$$

where EA(SiC) was determined to be 2.396(2) eV. The dissociation energy (D_0) indicates the difference between the dissociation energy limit of a diatomic molecule and the lowest vibrational energy level ($v = 0$), and the relationship between D_0 and the spectroscopic constants satisfies Eq. (2) (see the derivation in the Appendix). As a result, D_0(SiC) was calculated to be 5.089(11) eV based on the known spectroscopic constants of the neutral ground state ($X\ ^3\Pi$) for SiC,[28]

$$D_0 = \frac{\omega_e}{2}\left(\frac{1}{2x_e} - 1\right). \quad (2)$$

Furthermore, $D_0(SiC^-)$ was calculated to be 6.095(11) eV using Eq. (1). The fundamental vibrational frequency ν_0 of SiC^- in its electronic ground state ($X'\ ^2\Sigma^+$) is 1006(21) cm^{-1}. Within the framework of the Morse potential, the harmonic vibrational constant (ω_e)

TABLE III. Spectroscopic constants of anionic SiC^- and neutral SiC.

	Electronic state	Adiabatic excitation energy T_e (cm^{-1})	r_e (Å)	ω_e (cm^{-1})	$\omega_e x_e$ (cm^{-1})
SiC^-	$X'\,^2\Sigma^+$	0	1.69[a]	1016(21)	5.20(22)
	$A\,^2\Pi$	3380(101)	1.7449[b]	941(3)[c]	6(1)[c]
SiC	$X\,^3\Pi_2$	0	1.7182(2)[d]	964.768 61(20)[e]	5.603(12)[e]
	$a\,^1\Sigma^+$	5032(48)	1.6546[f]	1008[f]	⋯
	$b\,^1\Pi$	6737(38)	1.7277[f]	945[f]	⋯

[a]These values are from theoretical calculation.[47]
[b]These values are from theoretical calculation.[46]
[c]These values are from experiment.[48]
[d]These values are from experiment.[26]
[e]These values are from experiment.[28]
[f]These values are from theoretical calculation.[42]

and the anharmonic constant ($\omega_e x_e$) can be determined by Eqs. (3) and (4), yielding values of ω_e = 1016 ± 21 cm^{-1} and $\omega_e x_e$ = 5.20 ± 0.22 cm^{-1} for the ground state ($X'\,^2\Sigma^+$) of SiC^-,

$$\omega_e = \frac{2\nu_0 D_0}{2D_0 - \nu_0}, \tag{3}$$

$$\omega_e x_e = \frac{\omega_e \nu_0}{4D_0}. \tag{4}$$

These values are in reasonable agreement with previous theoretical predications.[46,47] The harmonic vibrational constant (ω_e) of the $X'\,^2\Sigma^+$ state was calculated to be 949.6 cm^{-1} at the CMRCI(0.01)+Q/aug-cc-pVDZ level,[46] while it was calculated to be 1127 cm^{-1} at the MP2(full)/6-311+G* level.[15] The harmonic vibrational constant (ω_e) was calculated to be 1013.4 cm^{-1} at the CMRCI(0.01)+Q/aug-cc-pV∞Z estimate level, which is the closest to the experimental measurement. Furthermore, the anharmonic constant ($\omega_e x_e$) of the $X'\,^2\Sigma^+$ state was calculated to be located between 4.5 and 6.21 cm^{-1}.[46] Based on the anionic and neutral spectroscopic constants summarized in Table III, the Morse potential energy curves for the $X'\,^2\Sigma^+$ and $A\,^2\Pi$ states of SiC^-, as well as the $X\,^3\Pi$, $a\,^1\Sigma^+$, and $b\,^1\Pi$ states of SiC, are plotted in Fig. 5. The solid lines represent SiC^-, while the dashed lines represent SiC. Based on these Morse potentials, a Franck–Condon factor (FCF) simulation for the overview cryo-SEVI spectra was performed using the PESCAL program.[74,75] As shown in Fig. 1(b), the FCF simulation supports our assignment.

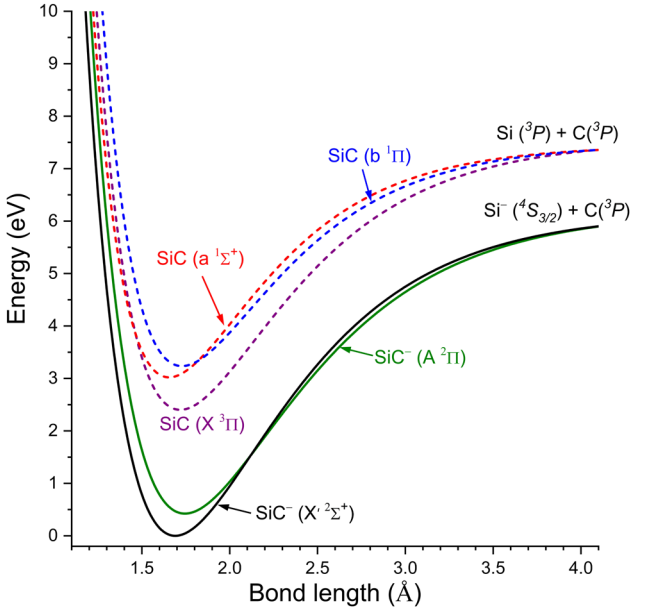

FIG. 5. Potential energy curves for the ground state of SiC^- ($X'\,^2\Sigma^+$), the electronically excited states of SiC^- ($A\,^2\Pi$), the neutral SiC ground state ($X\,^3\Pi$), and two electronically excited states ($a\,^1\Sigma^+$ and $b\,^1\Pi$).

In addition, the electronic absorption spectrum experiment shows that SiC^- in the neon matrix has another excited state B $^2\Sigma^+$, with 21 813(20) cm^{-1} above the anionic ground state $X'\,^2\Sigma^+$,[48] which is higher than EA(SiC) = 19 327(15) cm^{-1}. We did not find any other excited states of SiC^- in the gas phase near the EA by scanning the photon energy of the excitation laser.[76–78] Therefore, we believe that the proposed laser cooling transition $X'\,^2\Sigma^+ \leftrightarrow B\,^2\Sigma^+$ will result in a resonant autodetachment loss of SiC^-, suggesting that the SiC^- anion cannot be a potential candidate for laser cooling.

IV. CONCLUSIONS

In summary, high-resolution photoelectron spectra of cryogenically cooled SiC^- were obtained using the slow-electron velocity-map imaging (SEVI) method. Detailed vibrational progressions and fine structures corresponding to photodetachment transitions from the anionic ground state to the neutral ground and excited states were observed. The electron affinity (EA) of SiC was determined to be 19 327(15) cm^{-1} or 2.396(2) eV. In addition, a long-lived excited state of the SiC^- anion ($A\,^2\Pi$) was identified at 3380(101) cm^{-1} above its ground state ($X'\,^2\Sigma^+$). The spectroscopic constants of SiC^- were derived from the experimental data

and Morse potential curves. Moreover, our results indicate that SiC^- is not a suitable candidate for laser cooling of negative ions.

ACKNOWLEDGMENTS

This work was supported by the National Natural Science Foundation of China (NSFC) (Grant Nos. 12374244 and 12341401) and the Postdoctoral Fellowship Program of the CPSF (Grant No. GZC20231367).

AUTHOR DECLARATIONS

Conflict of Interest

The authors have no conflicts to disclose.

Author Contributions

S.Y. and J.C. contributed to the design and implementation of the research, S.Y. and J.C. to the analysis of the results, R.Z. and W.J. to the implementation and data analysis (support). C.N. supervised the project. S.Y. and C.N. wrote and reviewed the manuscript.

Shuaiting Yan: Conceptualization (lead); Formal analysis (lead); Investigation (lead); Writing – original draft (lead); Writing – review & editing (lead). **Jiayi Chen**: Data curation (equal); Formal analysis (equal); Investigation (equal). **Rui Zhang**: Data curation (equal); Formal analysis (equal); Investigation (equal). **Wenru Jie**: Data curation (equal); Formal analysis (equal); Investigation (equal). **Chuangang Ning**: Conceptualization (lead); Data curation (equal); Formal analysis (equal); Funding acquisition (lead); Investigation (equal); Supervision (lead); Writing – review & editing (supporting).

DATA AVAILABILITY

The data that support the findings of this study are available within this article.

APPENDIX: DERIVATION OF THE DISSOCIATION ENERGY D_0

1. Herzberg's method

Neglecting high-order terms ($\omega_e y_e$, $\omega_e z_e$, ...), the vibrational energy level $G(v)$ of the anharmonic oscillator is given by[79]

$$G(v) = \omega_e\left(v + \frac{1}{2}\right) - \omega_e x_e\left(v + \frac{1}{2}\right)^2. \tag{A1}$$

The energy interval between two adjacent vibrational energy levels is

$$\Delta G_{v+1/2} = G(v+1) - G(v) = \omega_e - 2\omega_e x_e - 2\omega_e x_e v. \tag{A2}$$

Thus, the fundamental vibrational frequency v_0 is

$$v_0 = \Delta G_{1/2} = \omega_e - 2\omega_e x_e. \tag{A3}$$

The exact expression for the vibrational frequency $v_{ose.}(v)$ that the anharmonic oscillator would have in the state v, according to classical theory, is

$$v_{ose.}(v) = c\Delta G_v. \tag{A4}$$

Here, it should be noted that ΔG_v not $\Delta G_{v+1/2}$ has to be used; that is, the vibrational frequency in the state v is intermediate between the two adjacent vibrational quanta $\Delta G_{v+1/2}$ and $\Delta G_{v-1/2}$. From Eqs. (A1) and (A2), we obtain

$$\Delta G_v = \frac{\Delta G_{v+1/2} + \Delta G_{v-1/2}}{2} = \frac{G(v+1) - G(v-1)}{2} = \omega_e - 2\omega_e x_e v - \omega_e x_e. \tag{A5}$$

Since no discrete vibrational levels lie above the asymptote when ΔG_v becomes zero, the maximum vibrational quantum v_D at the dissociation limit $\Delta G_v = 0$ is given by

$$v_D = \frac{1}{2x_e} - \frac{1}{2}. \tag{A6}$$

The highest of the asymptote (i.e., the beginning of the continuum) above the lowest vibrational level is equal to the work required to dissociate the molecule–the so-called dissociation energy (D_0), given by

$$D_0 = G(v_D) - G(0) = \frac{\omega_e}{4x_e} - \frac{\omega_e}{2} + \frac{\omega_e x_e}{4}. \tag{A7}$$

2. Morse potential and an alternative derivation of dissociation energy D_0

The Morse potential energy function is of the form[79,80]

$$U(r - r_e) = D_e\left(1 - e^{-\alpha(r-r_e)}\right)^2. \tag{A8}$$

Here, r is the distance between atoms, r_e is the equilibrium bond distance, and D_e is the well depth (defined relative to the dissociated atoms) and represents the dissociation limit, which can be calculated using the following relation:

$$D_e = D_0 + G(0). \tag{A9}$$

The parameter α controls the width of the potential (the smaller α is, the larger the well). It can be determined by

$$\alpha = \sqrt{\frac{2\pi^2 c\mu}{D_e h}}\omega_e = 1.2177 \times 10^7 \omega_e \sqrt{\frac{\mu_A}{D_e}}, \tag{A10}$$

where μ_A is the reduced mass in atomic-weight units and D_e is in cm^{-1}. The exact energy eigenvalues for the Morse potential are the same as in Eq. (A1).

An alternative definition for the dissociation limit was proposed by Yang and Chen, where the dissociation limit is determined using the vibrational energy interval $\Delta G_{v+1/2} = 0$, as above the dissociation energy, the spectrum tends to become continuous,[81]

$$\Delta G_{v+1/2} = G(v+1) - G(v) = \omega_e - 2\omega_e x_e - 2\omega_e x_e v = 0. \tag{A11}$$

From this equation, the maximum vibrational quantum v^* at the dissociation limit is given by

$$v^* = \frac{1}{2x_e} - 1. \tag{A12}$$

Thus, the dissociation energy (D_0) is given by

$$D_0 = G(v^*) - G(0) = \frac{\omega_e}{4x_e} - \frac{\omega_e}{2}. \tag{A13}$$

In the present work, we use Eq. (A13) to calculate the D_0 values. The slight difference $\omega_e x_e/4$ in the D_0 values between Eqs. (A7) and (A13) is due to the different definitions of the maximum vibrational quantum v at the dissociation limit. This difference $\omega_e x_e/4$ is neglectable compared to $\omega_e/4x_e$ in most cases. For example, $\omega_e x_e/4 = 1.3\ \mathrm{cm}^{-1}$ for the ground state $X'\,^2\Sigma^+$ of SiC^-, which is insignificant compared to $D_0(SiC^-) = 6.095(11)$eV.

REFERENCES

[1] H. Suzuki, Prog. Theor. Phys. **62**, 936 (1979).
[2] J. Cernicharo, C. A. Gottlieb, M. Guelin, P. Thaddeus, and J. M. Vrtilek, Astrophys. J. **341**, L25 (1989).
[3] R. Mollaaghababa, C. A. Gottlieb, J. M. Vrtilek, and P. Thaddeus, Astrophys. J. **352**, L21 (1990).
[4] T. Kimoto, Jpn. J. Appl. Phys. **54**, 040103 (2015).
[5] F. Roccaforte, P. Fiorenza, G. Greco, R. Lo Nigro, F. Giannazzo, F. Iucolano, and M. Saggio, Microelectron. Eng. **187-188**, 66 (2018).
[6] X. She, A. Q. Huang, Ó. Lucía, and B. Ozpineci, IEEE Trans. Ind. Electron. **64**, 8193 (2017).
[7] R. He, N. Zhou, K. Zhang, X. Zhang, L. Zhang, W. Wang, and D. Fang, J. Adv. Ceram. **10**, 637 (2021).
[8] X. Yin, L. Kong, L. Zhang, L. Cheng, N. Travitzky, and P. Greil, Int. Mater. Rev. **59**, 326 (2014).
[9] D. Cossart and M. Elhanine, Chem. Phys. Lett. **285**, 83 (1998).
[10] M. N. Deo and K. Kawaguchi, J. Mol. Spectrosc. **228**, 76 (2004).
[11] K. S. Ojha and R. Gopal, Spectrosc. Lett. **44**, 267 (2011).
[12] Y.-L. Yong, B. Song, J.-F. Li, and P.-M. He, J. Phys. B: At., Mol. Opt. Phys. **44**, 135101 (2011).
[13] Q.-X. Li, W.-C. Lu, Q.-J. Zang, L.-Z. Zhao, C. Z. Wang, and K. M. Ho, Comput. Theor. Chem. **963**, 439 (2011).
[14] J. M. L. Martin, J. P. Francois, and R. Gijbels, J. Chem. Phys. **92**, 6655 (1990).
[15] A. I. Boldyrev, J. Simons, V. G. Zakrzewski, and W. von Niessen, J. Phys. Chem. **98**, 1427 (1994).
[16] S. Hunsicker and R. O. Jones, J. Chem. Phys. **105**, 5048 (1996).
[17] P. Pradhan and A. K. Ray, J. Mol. Struct.: THEOCHEM **716**, 109 (2005).
[18] P. S. Yadav, R. K. Yadav, S. Agrawal, and B. K. Agrawal, Physica E **33**, 249 (2006).
[19] P. S. Yadav, R. K. Yadav, S. Agrawal, and B. K. Agrawal, J. Phys.: Condens. Matter **18**, 7085 (2006).
[20] S. Midda and A. K. Das, J. Mol. Struct.: THEOCHEM **633**, 67 (2003).
[21] C. M. Andreazza, R. M. Vichietti, and E. P. Marinho, Mon. Not. R. Astron. Soc. **400**, 1892 (2009).
[22] P. F. Bernath, S. A. Rogers, L. C. O'Brien, C. R. Brazier, and A. D. McLean, Phys. Rev. Lett. **60**, 197 (1988).
[23] C. R. Brazier, L. C. O'Brien, and P. F. Bernath, J. Chem. Phys. **91**, 7384 (1989).
[24] M. Ebben, M. Drabbels, and J. J. ter Meulen, Chem. Phys. Lett. **176**, 404 (1991).
[25] M. Ebben, M. Drabbels, and J. J. ter Meulen, J. Chem. Phys. **95**, 2292 (1991).
[26] T. J. Butenhoff and E. A. Rohlfing, J. Chem. Phys. **95**, 3939 (1991).
[27] R. Mollaaghababa, C. A. Gottlieb, and P. Thaddeus, J. Chem. Phys. **98**, 968 (1993).
[28] M. Wienkoop, P. Mürtz, P.-C. Schumann, M. Havenith, and W. Urban, Chem. Phys. **225**, 17 (1997).
[29] B. Gans, J. Liévin, P. Halvick, N. L. Chen, S. Boyé-Péronne, S. Hartweg, G. A. Garcia, and J. C. Loison, Phys. Chem. Chem. Phys. **25**, 23568 (2023).
[30] P. J. Bruna, S. D. Peyerimhoff, and R. J. Buenker, J. Chem. Phys. **72**, 5437 (1980).
[31] C. M. Rohlfing and R. L. Martin, J. Phys. Chem. **90**, 2043 (1986).
[32] C. W. Bauschlicher, Jr. and S. R. Langhoff, J. Chem. Phys. **87**, 2919 (1987).
[33] F. Müller-Plathe and L. Laaksonen, Chem. Phys. Lett. **160**, 175 (1989).
[34] S. R. Langhoff and C. W. Bauschlicher, Jr., J. Chem. Phys. **93**, 42 (1990).
[35] J. Deng, K. Su, Y. Zeng, X. Wang, Q. Zeng, L. Cheng, Y. Xu, and L. Zhang, Physica A **387**, 5440 (2008).
[36] W. Xing, D. Shi, and J. Sun, J. Quant. Spectrosc. Radiat. Transfer **227**, 86 (2019).
[37] B. L. Lutz and J. A. Ryan, Astrophys. J. **194**, 753 (1974).
[38] M. Larsson, J. Phys. B: At. Mol. Phys. **19**, L261 (1986).
[39] F. L. Sefyani and J. Schamps, Astrophys. J. **434**, 816 (1994).
[40] A. C. Borin, J. P. Gobbo, R. d. S. Batista, and L. G. M. de Macedo, Chem. Phys. **312**, 213 (2005).
[41] A. Pramanik and K. K. Das, J. Mol. Spectrosc. **244**, 13 (2007).
[42] D. H. Shi, W. Xing, J. F. Sun, and Z. L. Zhu, Eur. Phys. J. D **66**, 262 (2012).
[43] M. Zhang and K. Wang, J. Quant. Spectrosc. Radiat. Transfer **233**, 13 (2019).
[44] Q. Fan, H. Tian, Z. Fan, H. Li, J. Fu, J. Ma, and F. Xie, Spectrochim. Acta, Part A **287**, 122067 (2023).
[45] J. Anglada, P. J. Bruna, S. D. Peyerimhoff, and R. J. Buenker, J. Phys. B: At. Mol. Phys. **16**, 2469 (1983).
[46] Z.-L. Cai and J. P. François, J. Phys. Chem. A **103**, 1007 (1999).
[47] A. Pramanik, A. Banerjee, and K. K. Das, Chem. Phys. Lett. **468**, 124 (2009).
[48] M. Grutter, P. Freivogel, and J. P. Maier, J. Phys. Chem. A **101**, 275 (1997).
[49] P. Yzombard, M. Hamamda, S. Gerber, M. Doser, and D. Comparat, Phys. Rev. Lett. **114**, 213001 (2015).
[50] S. V. Shabanov and I. B. Gornushkin, Appl. Phys. A **122**, 676 (2016).
[51] X. Chen and C. Ning, Phys. Rev. A **93**, 052508 (2016).
[52] R. Tang, X. Fu, and C. Ning, J. Chem. Phys. **149**, 134304 (2018).
[53] R. Tang, X. Fu, Y. Lu, and C. Ning, J. Chem. Phys. **152**, 114303 (2020).
[54] W. C. Wiley and I. H. McLaren, Rev. Sci. Instrum. **26**, 1150 (1955).
[55] A. T. J. B. Eppink and D. H. Parker, Rev. Sci. Instrum. **68**, 3477 (1997).
[56] A. Kasdan, E. Herbst, and W. C. Lineberger, J. Chem. Phys. **62**, 541 (1975).
[57] W. Chaibi, R. J. Peláez, C. Blondel, C. Drag, and C. Delsart, Eur. Phys. J. D **58**, 29 (2010).
[58] C. Ning and Y. Lu, J. Phys. Chem. Ref. Data **51**, 021502 (2022).
[59] S. Yan, Y. Lu, R. Zhang, and C. Ning, Chin. J. Chem. Phys. **37**, 1 (2024).
[60] K. M. Ervin, J. Ho, and W. C. Lineberger, J. Phys. Chem. **92**, 5405 (1988).
[61] A. Delon and R. Jost, J. Chem. Phys. **95**, 5686 (1991).
[62] Y. Zheng and S. Ding, Int. J. Quantum Chem. **108**, 1059 (2008).
[63] S. Ndengué, E. Quintas-Sánchez, R. Dawes, and D. Osborn, J. Phys. Chem. A **125**, 5519 (2021).
[64] B. Dick, Phys. Chem. Chem. Phys. **16**, 570 (2014).
[65] C. Lee, W. Yang, and R. G. Parr, Phys. Rev. B **37**, 785 (1988).
[66] A. D. Becke, J. Chem. Phys. **98**, 5648 (1993).
[67] R. Krishnan, J. S. Binkley, R. Seeger, and J. A. Pople, J. Chem. Phys. **72**, 650 (1980).
[68] See http://www.gaussian.com for Gaussian program, Gaussian, Wallingford CT, 2004.
[69] W. Humphrey, A. Dalke, and K. Schulten, J. Mol. Graphics **14**, 33 (1996).
[70] A. Sanov and R. Mabbs, Int. Rev. Phys. Chem. **27**, 53 (2008).
[71] E. Garand, K. Klein, J. F. Stanton, J. Zhou, T. I. Yacovitch, and D. M. Neumark, J. Phys. Chem. A **114**, 1374 (2010).
[72] Y. Liu and C. Ning, J. Chem. Phys. **143**, 144310 (2015).
[73] D. Bresteau, C. Drag, and C. Blondel, Phys. Rev. A **93**, 013414 (2016).
[74] K. M. Ervin and W. C. Lineberger, PESCAL, Fortran program, 2010.
[75] M. L. Polak, G. Gerber, J. Ho, and W. C. Lineberger, J. Chem. Phys. **97**, 8990 (1992).
[76] S. Yan, R. Zhang, Y. Lu, and C. Ning, J. Chem. Phys. **160**, 064303 (2024).

[77]R. Tang, R. Si, Z. Fei, X. Fu, Y. Lu, T. Brage, H. Liu, C. Chen, and C. Ning, Phys. Rev. A **103**, 042817 (2021).
[78]Y. Lu, R. Zhang, C. Song, C. Chen, R. Si, and C. Ning, Chin. Phys. Lett. **40**, 093101 (2023).
[79]G. Herzberg, *Molecular Spectra and Molecular Structure: I. Spectra of Diatomic Molecules* (Van Nostrand, New York, 1950).
[80]P. M. Morse, Phys. Rev. **34**, 57 (1929).
[81]G. Yang and S. Chen, J. Northeast Norm. Univ. **36**, 50 (2004).